How to cite: *Angew. Chem. Int. Ed.* **2025**, e202513522
doi.org/10.1002/anie.202513522

Cobalt Catalysis **Hot Paper**

A Homobimetallic Frustrated Lewis Pair Cobalt Catalyst for the Methanolysis of Hydrosilanes

Ana Luque-Gómez, Daniel Barrena-Espés, Pilar García-Orduña, Andrea Pérez-García, Miguel A. Casado, Julen Munarriz, and Manuel Iglesias**

Dedicated to Prof. Luis A. Oro on the occasion of his 80th birthday

Abstract: The bimetallic Co(I)/Co(–I) complex $[Co(CO)_2(\kappa^3\text{-}P,N,P\text{-}PN^HP)][Co(CO)_4]$ (**1**) has shown excellent activities in the methanolysis of hydrosilanes, surpassing the related bimetallic Co(I)/Co(–I) complex $[Co(CO)(PMe_2Ph)(\kappa^3\text{-}P,N,P\text{-}PN^HP)][Co(CO)_4]$ (**2**), the Co(II) complex $[Co(Cl)_2(\kappa^3\text{-}P,N,P\text{-}PN^HP)]$ (**3**), and the Co(I) complex $[Co(CO)_2(\kappa^3\text{-}P,N,P\text{-}PN^HP)]Cl$ (**4**). A comprehensive DFT study of the plausible reaction mechanisms indicates that the enhanced activity of **1** can be attributed to the presence of the $[Co(CO)_4]^-$ anion, which enables a frustrated Lewis pair (FLP) mechanism that provides a low energy pathway for the heterolytic splitting of the Si—H bond. The reaction mechanism entails the coordination of the hydrosilane to the Co(I) center upon decoordination of the amine functionality of the PN^HP ligand, followed by heterolytic splitting of the Si—H bond with the participation of the Co(I) and Co(–I) centers. Then, the $PhSiH_2$ group at the Co(–I) center is transferred to the oxygen atom of a methanol molecule, which affords the $[H_2SiPh(HOMe)]^+$ cation, regenerating the $[Co(CO)_4]^-$ species. $[H_2SiPh(HOMe)]^+$ protonates the hydride at the Co(I) center, leading to the formation of H_2 and the corresponding silyl ether. Alternative reaction pathways, including alternative ionic mechanisms or NH-assisted bifunctional mechanisms, result in higher activation energies.

Introduction

The synthesis of silanols, siloxanes, and alkoxysilanes is of paramount significance in organosilicon chemistry, allowing for the preparation of diverse silicon-based materials, including elastomers, resins, and adhesives.[1–4] As an alternative to stoichiometric methods, in the presence of suitable catalysts, hydrosilanes undergo the dehydrogenative hydrolysis or alcoholysis of the Si—H bond(s) under mild conditions, thus leading to the formation of silanols or siloxanes in the case of the former, and alkoxysilanes in the case of the latter.

The generation of hydrogen as a coproduct in both reactions, together with the low toxicity and kinetic stability of organosilanes, has prompted the exploration of hydrosilanes as hydrogen storage systems.[5] Examples of heterogeneous catalysts for hydrogen generation from hydrosilanes by hydrolysis or methanolysis have been described.[6–13] However, their homogeneous counterparts based on precious metal complexes have been the most successful so far—especially those featuring iridium centers.[14–19] Conversely, there is a dearth of reports on homogeneous catalysts that rely on Earth-abundant metals (EAMs) for these transformations. Among them, cobalt catalysts have been the most prolific. In this regard, it is remarkable that only Co(II) catalysts have been reported, which contrasts with the fact that Co(I) complexes are frequently described as the active species, either as well-defined or as in situ generated catalysts.[20–30]

Noteworthy examples of cobalt catalysts for the hydrolysis and methanolysis of hydrosilanes are those depicted in Figure 1. Catalyst **I**, reported by Pattanaik et al., efficiently promotes the selective formation of disiloxanes and hydrodisiloxanes from hydrosilanes and silanols in the presence of catalytic amounts of K^{t}BuO. The reaction of K^{t}BuO with **I** has been proposed to generate an unsaturated Co(II) complex that acts as the active species upon deprotonation of the NH moieties of its pincer ligand.[31] The oxidation state of the cobalt center is maintained throughout the postulated catalytic cycle, which would proceed by an outer-sphere mechanism that entails the nucleophilic attack of

[*] Dr. A. Luque-Gómez, Dr. P. García-Orduña, A. Pérez-García, M. A. Casado, Dr. M. Iglesias
Instituto de Síntesis Química y Catálisis Homogénea, CSIC-Universidad de Zaragoza, C/Pedro Cerbuna 12, Facultad de Ciencias, Zaragoza 50009, Spain
E-mail: miglesia@unizar.es

D. Barrena-Espés
Departamento de Química Física y Analítica, Universidad de Oviedo, Avda. Julián Clavería 8, Oviedo 33006, Spain

Dr. J. Munarriz
Departamento de Química Física and Instituto de Biocomputación y Física de Sistemas Complejos (BIFI), Universidad de Zaragoza, C/Pedro Cerbuna 12, Facultad de Ciencias, Zaragoza 50009, Spain
E-mail: julen@unizar.es

Additional supporting information can be found online in the Supporting Information section

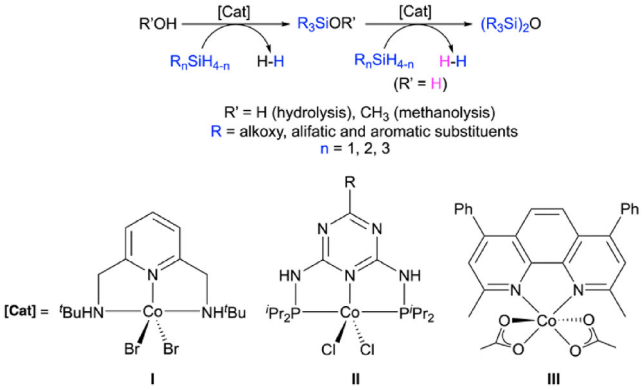

Figure 1. Depiction of cobalt catalysts for the dehydrogenative alcoholysis or hydrolysis of silanes.

the oxygen atom of the silanol or water over the silicon center of a coordinated hydrosilane. This catalytic cycle is reminiscent of the electrophilic mechanism originally proposed by Luo and Crabtree for Ir-catalysts,[15] and later supported by mechanistic studies on other Ir-systems.[14,32] Catalyst **II** was successfully employed for the synthesis of monohydrosilyl ethers by reaction of di- and tri-hydrosilanes with a variety of alcohols in excellent selectivities.[33] In contrast with **I**, the catalytic cycle proposed for **II** entails the in situ formation of a Co(I) species, which, upon oxidative addition of the hydrosilane's Si–H bond, affords a Co(III) dihydride intermediate. Protonation of one of the hydride ligands by the alcohol generates a molecule of H_2 and an alkoxide complex. Subsequent reductive elimination yields the silyl ether and regenerates the Co(I) species. The Co(II) complex **III** reported by Guo et al.—although isolated and characterized by the authors—is formed in situ by reaction of $Co(OAc)_2$ with the functionalized phenanthroline ligand. Selective hydrolysis and alcoholysis of monohydrosilanes has been achieved with **III** and other catalysts featuring related phenanthrolines.[34]

Other EAM-catalysts able promote this type of reactions, based on Mn,[35,36] Fe[37] or Zn,[38] have been reported. Although the use of these EAM-based catalysts for the synthesis of siloxanes, silanols, and alkoxysilanes has been studied, their H_2-production capabilities, especially in the case of cobalt catalysts, have received less attention. In this regard, it is worth noting that the use of organosilanes that contain multiple Si–H bonds, such as $C(SiH_3)_4$, *cyclo*$(CH_2SiH_2CHSiH_3)_2$ or *cyclo*-$(CH_2SiH_2)_3$,[5] present high gravimetric hydrogen capacities, in the range or above the 5.5 wt% target set by US Department of Energy. Therefore, di- and tri-hydrosilanes could be considered suitable models for the study of on-demand hydrogen production.

A promising strategy for enhancing the activity of transition metal catalysts, particularly those based on EAMs, involves the design of bifunctional catalysts that operate through metal–metal or metal–ligand cooperation. Prominent examples of the latter entail the use of MACHO-type ligands, $HN(CH_2CH_2PR_2)_2$, which have shown excellent performances in (de)hydrogenation reactions catalyzed by transition metal complexes—with the Ru-MACHO catalyst being a notorious example.[39–43] The activity of complexes containing MACHO ligands has often been attributed to the role played by the metal-bound NH moiety, which is capable of prompting Noyori-type mechanisms.[44] The use of these ligands has enabled the development of efficient dehydrogenation catalysts based on EAMs. Representative examples of this reactivity are Fe,[45,46] Mn,[47] and Co[48] catalysts for the dehydrogenation of methanol and formic acid.

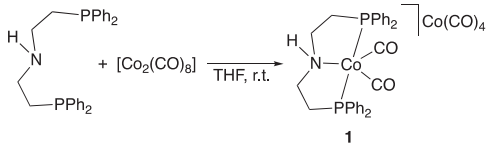

Scheme 1. Synthesis of complex **1**.

In this work, we have assessed the performance of several cobalt MACHO-type catalysts in the dehydrogenative methanolysis of hydrosilane model compounds, such as Ph_2SiH_2 and $PhSiH_3$. Additionally, we explored the reaction mechanisms that operate in these reactions by experimental methods and DFT calculations. Our study points to the presence of two novel divergent reaction mechanisms for the Co(I)/Co(–I) and Co(II) precatalysts.

Results and Discussion

Synthesis and Characterization of Cobalt Catalysts

Based on previous work by us on the synthesis of Co(I)/Co(–I) bimetallic complexes,[49] we initially explored the reaction of $HN(CH_2CH_2PPh_2)_2$ (PN^HP) with 1 equiv of $[Co_2(CO)_8]$ (Scheme 1), which straightforwardly allowed us to prepare complex $[Co(CO)_2(\kappa^3\text{-}P,N,P\text{-}PN^HP)][Co(CO)_4]$ (**1**).

Complex **1** is diamagnetic, which allowed for its characterization in solution by NMR spectroscopy. The ^1H NMR spectrum in C_6D_6 shows three low-field signals at δ 7.52–6.50 ppm that correspond to the protons of the aromatic rings. A broad singlet at δ 5.20 ppm that integrates 1H can be assigned to the NH, which was confirmed by the ^1H-^{15}N HMQC NMR spectrum. The remaining four resonances, at δ 3.20, 2.50, 2.19, and 1.78 ppm, can be assigned to the protons of the NCH_2 and PCH_2 groups, which become diastereotopic upon coordination. The $^{13}C\{^1H\}$-APT NMR spectrum shows, as the most representative signals, two overlapping triplets at δ 198.6–197.7 ppm that belong to the two CO ligands at the cation coupled with the two ^{31}P nuclei. Furthermore, at δ 34.9 ppm, an apparent triplet appears due to the coupling of the PCH_2 carbon atom with the two ^{31}P nuclei. The ^1H-^{13}C HSQC spectrum allowed us to assign each of the ^1H NMR signals. The CH_2P peak at δ 34.9 ppm in the $^{13}C\{^1H\}$-APT NMR shows correlations with the resonances at δ 2.50 and 2.19 ppm in the ^1H NMR, which are assigned to the PCH_2 groups. On the other hand, the signals at δ 3.20 and 1.78 ppm show correlations with a singlet at δ 53.2 ppm in the $^{13}C\{^1H\}$-APT NMR spectrum, and are therefore attributed to the NCH_2 groups.

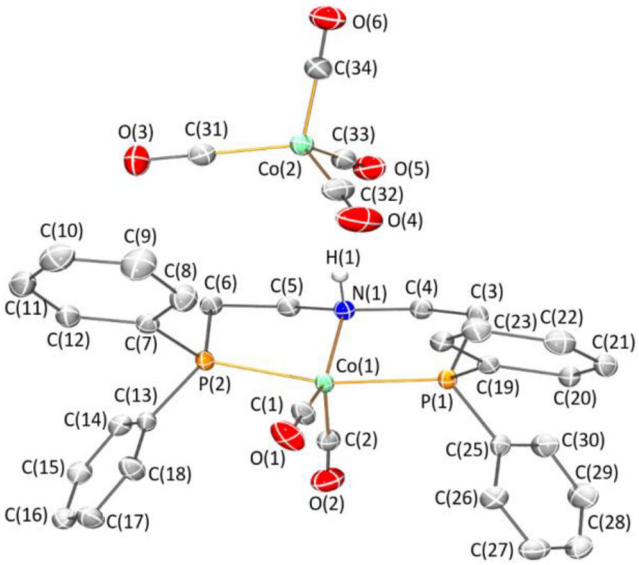

Figure 2. Molecular structure of **1** with ellipsoids at 50% probability. Hydrogen atoms (except that of NH group) and a cocrystallized toluene molecule have been omitted for clarity. Selected bonds lengths (Å) and angles (°): Co(1)-P(1) 2.1950(6), Co(1)-P(2) 2.1880(6), Co(1)-N(1) 2.0586(17), Co(1)-C(1) 1.729(2), Co(1)-C(2) 1.816(2), Co2-C31 1.773(2), Co2-C32 1.762(2), Co2-C33 1.776(2), and Co2-C34 1.770(2); P(1)-Co(1)-P(2) 163.88(3), P(1)-Co(1)-N(1) 85.80(5), P(1)-Co(1)-C(1) 91.06(7), P(1)-Co(1)-C(2) 98.13(7), P(2)-Co(1)-N(1) 84.31(5), P(2)-Co(1)-C(1) 90.69(7), P(2)-Co(1)-C(2) 96.18(7), N(1)-Co(1)-C(1) 148.29(10), N(1)-Co(1)-C(2) 100.66(9), C(1)-Co(1)-C(2) 111.02(11) C(31)-Co(2)-C(33) 112.53(10), C(32)-Co(2)-C(31) 106.97(11), C(32)-Co(2)-C(33) 114.24(12), C(32)-Co(2)-C(34) 106.92(11), and C(34)-Co(2)-C(31) 106.38(11) y C(34)-Co(2)-C(33) 109.36(11).

The $^{31}P\{^{1}H\}$ NMR spectrum shows a singlet at δ 70.3 ppm, as both ^{31}P nuclei are equivalent due to the symmetry plane containing the N, Co, and the two carbonyl ligands.

The FTIR spectrum shows two bands at 2005 and 1942 cm^{-1}, attributed to the two carbonyl ligands attached to the Co(I) center, and an intense band at 1865 cm^{-1} that corresponds to the $[Co(CO)_4]^-$ anion.

Crystals of **1** suitable for single-crystal X-ray diffraction were obtained by slow diffusion of hexane into a toluene solution of the complex (Figure 2). The geometry of the cation can be described as a distorted square pyramid (τ = 0.26),[50] with P(1)-Co(1)-P(2) and N(1)-Co(1)-C(1) angles of 163.88(5)° and 148.29(10)°, respectively. The tridentate-coordinated PN^HP ligand occupies three positions at the base of the pyramid, while the two carbonyl ligands occupy the remaining basal and apical positions. Geometrical parameters characterizing the cobalt center nicely agree with those found in related cobalt complexes with PN^HP pincer ligands, such as $MeN[CH_2CH_2(P^iPr_2)]_2$ or, specially, $HN[CH_2CH_2(PCy_2)]_2$.[51]

The $[Co(CO)_4]^-$ counterion presents a distorted tetrahedral structure, with angles that significantly deviate from the 109° expected for an ideal geometry. This can be attributed to a weak hydrogen bond interaction between the Co(2) atom and the NH of the PN^HP ligand coordinated to Co(1), which highlights the Lewis basic character of the Co(–I) center.

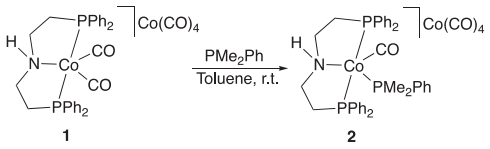

Scheme 2. Synthesis of complex **2**.

It is noteworthy that geometric parameters [N(1)···Co(2): 3.9343(15) Å, H(1)···Co(2): 3.07(3) Å, and N(1)-H(1)···Co(2): 161(3)°] pointed out that this intermolecular interaction is weaker than N–H···Co hydrogen bonds between carbonyl-cobaltate anions and NH groups that have been previously described in the literature.[52,53]

Complex **1** was reacted with PMe_2Ph in order to evaluate the lability of the carbonyl ligands and, consequently, its ability to generate a vacant coordination site. The addition of PMe_2Ph to a solution of **1** in toluene causes substantial gas evolution due to CO loss. However, the reaction is sluggish and needs to be performed in an open system to proceed to completion, affording **2**, $[Co(CO)(PMe_2Ph)(\kappa^3\text{-}P,N,P\text{-}PN^HP)][Co(CO)_4]$, as the only metal species (Scheme 2). Encouraged by this result, we also evaluated the reactivity of **1** with other Lewis bases. Initially, we explored the addition of an excess of pyridine, which resulted only in the formation of trace amounts of an unidentified complex over extended reaction times. Similar behavior was observed with $PMePh_2$ and $Ph_3P{=}O$. We also explored the use of Me_3NO to abstract a CO ligand in the presence of py, but no measurable reaction was observed. This suggests that CO substitution in **1** is possible but not straightforward.

The coordination of the PMe_2Ph ligand was confirmed by $^{31}P\{^{1}H\}$ NMR, which displays a doublet and a triplet at δ 56.6 and −4.9 ppm, respectively, with coupling constants of 83.8 Hz. The presence of one carbonyl ligand was corroborated by the observation of a multiplet at δ 214.9–214.3 ppm in the $^{13}C\{^{1}H\}$ NMR spectrum. Moreover, the FTIR spectrum shows only one band at 1934 cm^{-1} for the only carbonyl ligand and an intense band at 1856 cm^{-1} for the $[Co(CO)_4]^-$ anion.

The fact that the only Co catalysts hitherto reported for the hydrolysis or methanolysis of silanes were based on Co^{II} centers, prompted us to prepare $[Co(Cl)_2(\kappa^3\text{-}P,N,P\text{-}PN^HP)]$[54] (**3**) for comparison purposes. Inspired by Szafoni's work,[33] we envisaged that the reaction of **3** with hydrosilane would lead to the in situ formation of a $Co^I(\kappa^3\text{-}P,N,P\text{-}PN^HP)$ species without the strongly coordinating carbonyl ligands present in **1** or **2**, thus allowing easy access of the substrates to the metal center.

The reactivity of **3** with stoichiometric amounts of hydrosilanes was explored in order to shed light on whether or not in situ reduction to a Co^I catalyst takes place. In a Young NMR tube, 3 equiv of $PhSiH_3$ was added to a dark purple solution of **3** in CD_3CN, causing a color change to yellow-green at room temperature over a period of ca. 30 min. This process was accompanied by copious gas evolution. During this period, the presence of paramagnetic Co(II) species prevented the monitoring of the reaction by NMR. Then, a mixture of diamagnetic hydride complexes (δ ca. −20 to

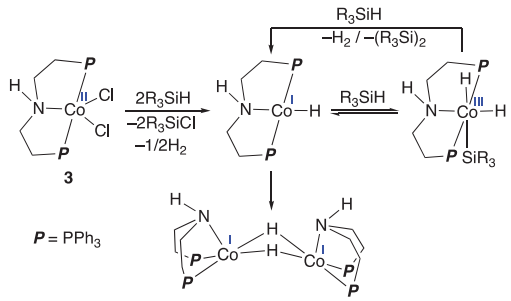

Scheme 3. Proposed reactivity of **3** with a generic hydrosilane.

−23 ppm) is observed in the ^{1}H NMR, accompanied by a hydrogen peak. The ^{1}H NMR data suggests initial formation of a monohydride from **3**, which undergoes oxidative addition of a molecule of hydrosilane to yield a Co(III) complex. Upon reaction with a new molecule of hydrosilane, the dihydride species would react with a molecule of hydrosilane via dehydrogenative coupling. This is supported by the observation of silane dimerization and oligomerization peaks[49,55,56] in the ^{1}H NMR between δ 5.05 and 5.25 ppm, and the fact that H_2 evolution continues throughout the reaction, eventually leading to consumption of all the excess of $PhSiH_3$. Once all the $PhSiH_3$ has been consumed, the monohydride species dimerizes to afford a dinuclear complex that features, tentatively, two bridging hydride ligands. This would explain the appearance of the resonance at ca. δ −11 ppm in the ^{1}H NMR (Scheme 3). A more detailed discussion has been included in the Supporting Information.

Evaluation of the Catalytic Activity

The initial exploration of the catalytic activity focused on the methanolysis of $PhSiH_3$ using complexes **1**, **2,** and **3** as catalysts. The reactions were carried out in a reactor equipped with a pressure transducer (Man on the Moon series X102). This setup enabled us to monitor the progress of the reaction by measuring the amount of hydrogen gas generated in the process. Full conversion was achieved using MeOH as solvent and reactant, at 50 °C, with $PhSiH_3$ and 1 mol% catalyst loading. At variance with the other reports on cobalt catalysts for this transformation,[31,33] the three Si─H bonds of the trihydrosilane, $PhSiH_3$, were converted into Si─O bonds to afford $PhSi(OMe)_3$ with catalysts **1**, **2,** and **3**. Nonetheless, it is worth mentioning that the methanolysis of the Si─H bond of the intermediate species $PhSi(OMe)_2H$ is more sluggish than that of the previous two ($PhSiH_3$ and $PhSi(OMe)H_2$), which can be detected as a noticeable change of slope at around a 66% conversion, especially in the case of catalyst **2** (Figure 3). The reactivity of $PhSiH_3$ and the intermediate hydrosilanes is expected to follow the trend $PhSiH_3$ > $PhSi(OMe)H_2$ > $PhSi(OMe)_2H$ > $PhSi(OMe)_3$. Although the difference in reactivity between $PhSiH_3$ and $PhSi(OMe)H_2$ is less evident than that between $PhSi(OMe)H_2$ and $PhSi(OMe)_2H$, this behavior can also be detected (Figure S24). Catalysts **1** showed the best overall performance, reaching full conversion after ca. 5 min.,

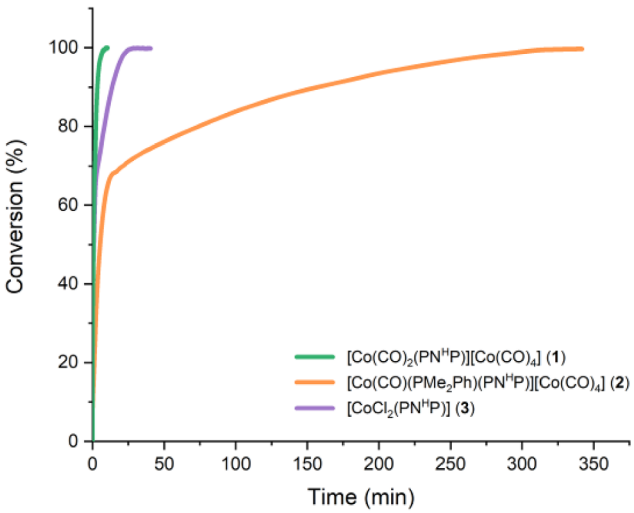

Figure 3. Conversion over time for the methanolysis of $PhSiH_3$ (0.5 mmol) at 50 °C in MeOH (0.5 mL) with of catalysts **1**, **2**, and **3** (1 mol%).

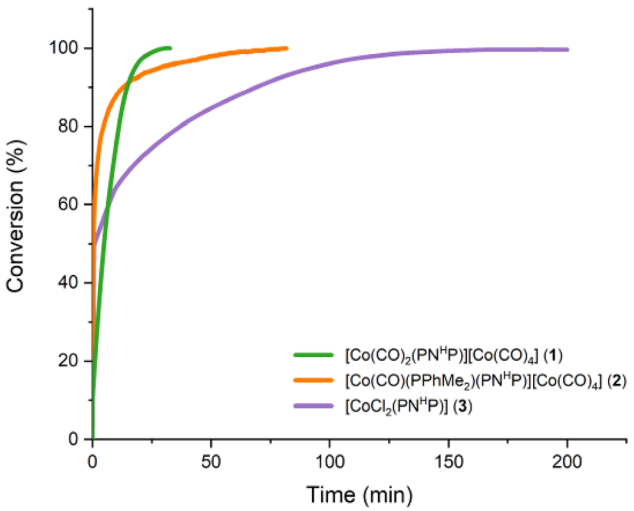

Figure 4. Conversion over time for the methanolysis of Ph_2SiH_2 (0.5 mmol) at 50 °C in MeOH (0.5 mL) with of catalysts **1**, **2**, and **3** (1 mol%).

followed by **3**, which is less active for the methanolysis of $PhSi(OMe)_2H$, and requires ca. 25 min to reach full conversion. Finally, **2** stands as the least active catalyst within the series, mainly due to the low activity in the methanolysis of intermediate monohydrosilane $PhSi(OMe)_2H$. Initial TOFs were calculated, resulting in values of 41 970 , 4478, and 28 234 h^{-1} for **1**, **2**, and **3**, respectively. This confirms that the reaction times required to achieve full conversion are consistent with the initial TOF values.

The proficiency of these catalysts for the methanolysis of the intermediate dihydrosilane prompted us to investigate the use of Ph_2SiH_2 as substrate (Figure 4).

To our surprise, we observed a substantial change in the activity trend. Although **1** is still the fastest catalyst to achieve full conversion, **2** and **3** are more active in the initial stages

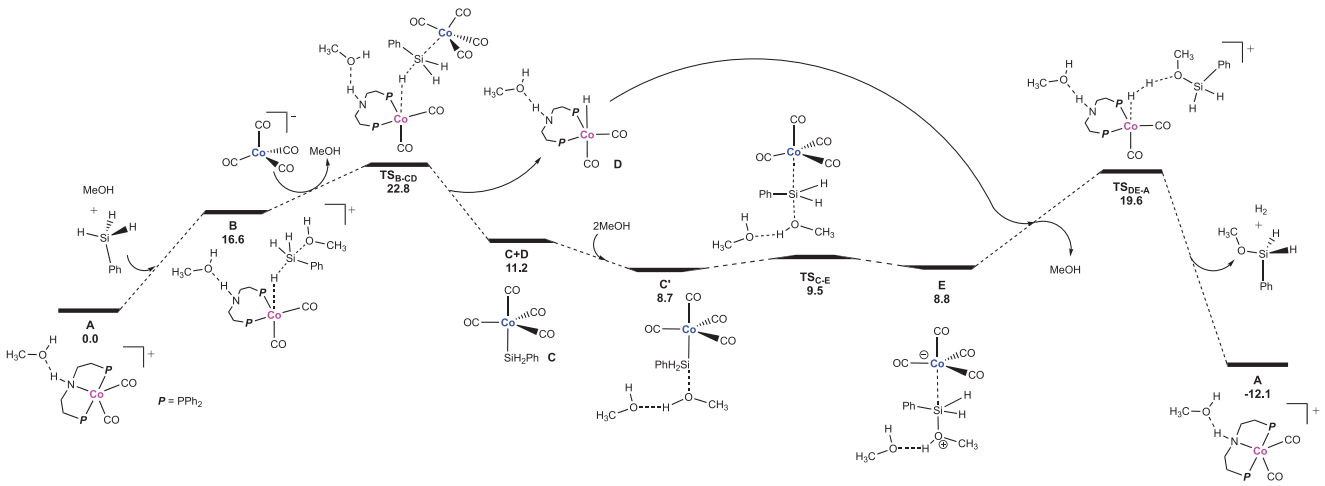

Figure 5. DFT calculated Gibbs energy profile for the methanolysis of $PhSiH_3$ (in kcal·mol^{-1}) relative to **A**.

of the reaction, with initial TOF values of 4040, 49 570 and 3310 h^{-1} for **1**, **2**, and **3**, respectively. This could be attributed to the fact that **1** reacts with Ph_2SiH_2 and $Ph_2Si(OMe)H$ almost simultaneously, while the reactions catalyzed by **2** or **3** occur in a more stepwise manner, consuming first Ph_2SiH_2 and subsequently the less reactive $Ph_2Si(OMe)H$. This behavior, denoted by a noticeable decrease of the slope after 50% conversion, is especially manifested in the case of **3**.

Lastly, we studied the reactivity of the monohydrosilanes Ph_2MeSiH and $PhMe_2SiH$. None of the catalysts showed activity for the former, while the methanolysis of the latter was only catalyzed by **3** (Figure S25).

Mechanistic Studies

In order to attain a deeper understanding of the reaction mechanisms and unravel the behavior observed for catalysts **1** and **3**, a DFT examination of various plausible pathways was carried out (see Computational Details in the Electronic Supporting Information for additional information). We found that the most favorable reaction mechanism for **1** is that provided in Figure 5. For the sake of clarity, reaction intermediates are referred to by capital letters starting from **A**, which coincides with **1** stabilized by a molecule of methanol (which was added to take into account the hydrogen bond formation between the solvent and the H atom of the NH group in the PN^{H}P ligand).

This mechanism is related to ionic outer-sphere mechanisms[57–66] or the mechanism proposed by Luo and Crabtree for the alkoholysis of silanes;[15] however, in this case, the heterolytic splitting of the Si–H bond involves the collaboration of the $[Co(CO)_4]^-$ anion instead of MeOH. In this regard, we note that the nucleophilicity of $[Co(CO)_4]^-$ and its ensuing capacity to participate in bifunctional mechanisms have been reported in the literature, particularly in the catalytic functionalization of epoxides.[67–70] These catalysts are usually based on ion pairs that comprise a Lewis acid center and the Lewis basic $[Co(CO)_4]^-$ anion, with the latter acting as a nucleophile that opens the epoxide ring.

The reaction starts by coordination of the hydrosilane to the Co(I) center in **A**, yielding intermediate **B** upon decoordination of the amine functionality in the PN^{H}P ligand. Such intermediate is also stabilized by an additional methanol molecule, and bears a relative Gibbs energy of 16.6 kcal·mol^{-1}. Then, the hydrosilane is activated by a cooperative mechanism that involves the participation of the $[Co(CO)_4]^-$ counterion. For that, there should first be a ligand exchange between methanol and $[Co(CO)_4]^-$, leading to a Gibbs energy increase of 2.6 kcal·mol^{-1} (structure B-$[Co(CO)_4]$, provided in the Supporting Information). The reaction then proceeds through a cooperative mechanism via $\mathbf{TS_{B\text{-}CD}}$ (Figure 6a), involving a nucleophilic attack of the cobaltate anion to the silicon atom with concomitant hydride abstraction by the Co(I) center. This process requires surmounting a Gibbs energy barrier of 22.8 kcal·mol^{-1} (dictated by the difference between $\mathbf{TS_{B\text{-}CD}}$ and **A**) and leads to the formation of intermediates **C** and **D**, with a relative Gibbs energy of 11.2 kcal·mol^{-1}. **C** corresponds to the silylated analogue of $[Co(CO)_4]^-$, while **D** is a Co(I)-based hydride intermediate, and will be relevant in subsequent steps.

The next reaction step involves the interaction of a methanol molecule with the silicon atom of **C**—which also establishes a hydrogen bond with an additional methanol molecule—yielding **C'**, with a relative Gibbs energy of 8.7 kcal·mol^{-1} (2.5 kcal·mol^{-1} more stable than **C**). The $PhSiH_2$ group in **C'** can be then transferred to the oxygen atom of methanol, which is easily achieved via $\mathbf{TS_{C\text{-}E}}$ (see Figure 6b)—the energy barrier is only 0.8 kcal·mol^{-1}, producing **E**, with a relative Gibbs energy of 8.8 kcal·mol^{-1} (only 0.1 kcal·mol^{-1} less stable than **C'**). Such process involves the regeneration of the $[Co(CO)_4]^-$ species, and the formation of the $[H_2SiPh(HOMe)]^+$ cation, in which the Si–O bond of the final product has already been formed. The last step of the catalytic cycle consists of the protonation of the hydride ligand in **D** by the cation $[H_2SiPh(HOMe)]^+$, yielding molecular hydrogen, $H_2SiPh(OMe)$, and regenerating **A**. This step requires surmounting $\mathbf{TS_{DE\text{-}A}}$, with a relative Gibbs energy of 19.6 kcal·mol^{-1} (that is, it is 10.8 kcal·mol^{-1} higher in Gibbs energy than **E**). Noteworthy, while all the other reaction steps

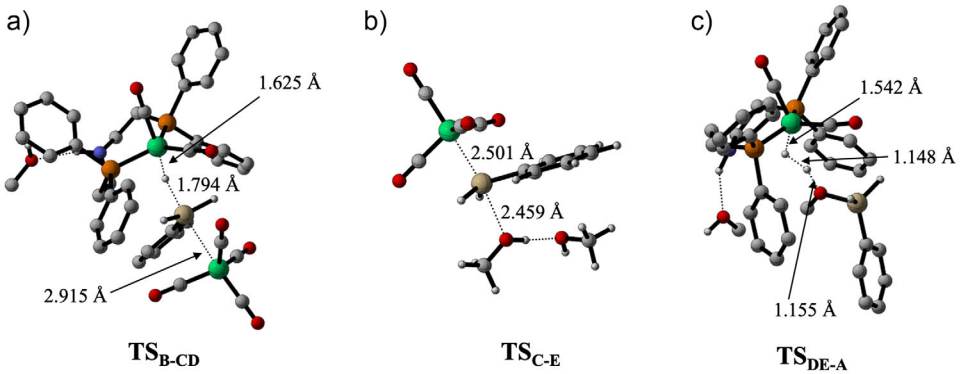

Figure 6. DFT-optimized structures and selected distances of a) $\mathbf{TS_{B\text{-}CD}}$, b) $\mathbf{TS_{C\text{-}E}}$, and c) $\mathbf{TS_{DE\text{-}A}}$. Notice that nonrelevant hydrogen atoms in a) and c) have been omitted for clarity.

can be considered to be reversible (the direct and inverse processes take place with relatively low energy barriers), this one is virtually irreversible, as the products have a relative Gibbs energy of −12.1 kcal·mol^{-1}, which leads to an energy barrier for the inverse process of 31.7 kcal·mol^{-1}. In addition, the H_2 molecule has a low solubility in methanol, and is thus expected to leave the solution.

Overall, the Gibbs energy variation of the reaction is −12.1 kcal·mol^{-1} and the effective energy span is 22.8 kcal·mol^{-1}, being determined by the activation of the H−Si bond ($\mathbf{TS_{B\text{-}CD}}$). This result is in agreement with experimental observations—reaction temperature and KIE experiments (vide infra).

At this point, we note that complex **2**, which features a phosphine ligand replacing a CO ligand (see above), is expected to exhibit a more challenging activation of the hydrosilane molecule (via $\mathbf{TS_{B\text{-}CD}}$). Broadly speaking, this is due to the more basic nature of the phosphine ligand compared to CO, which donates greater electron density to the metal center. This increased electron richness at the metal hinders hydride abstraction (required for hydrosilane activation), ultimately leading to a higher activation Gibbs energy, in agreement with the significantly poorer performance of **2** with respect to **1**.

Other potential mechanisms, alternative to the Co(I)/Co(–I) bifunctional activation, have been considered. Namely, the Luo-Crabtree mechanism was calculated (see Figure 7a for the first part and Figure S26 for the whole mechanism). The first step (Figure 7a, black lines) consists of the MeOH-assisted Si–H bond cleavage via $\mathbf{TS_{B\text{-}DF}}$ (Figure 7b). This step is also the rate-determining one, and involves an energy span of 27.2 kcal·mol^{-1}, which is 4.4 kcal·mol^{-1} higher than the cobaltate-assisted one. Note that the following reaction stages entails the hydride protonation by **F** to yield H_2, the corresponding methoxysilane, and **A** by means of $\mathbf{TS_{D\text{-}A}}$ (Figure S27).

Another potential alternative involves the active participation of the amine functionality of the pincer scaffold (see Figure 7b, blue lines). In this case, the silane activation would proceed in a concerted manner, as dictated by $\mathbf{TS_{B\text{-}G}}$ (Figure 7c), yielding the methoxysilane and a hydride intermediate (**G**), featuring a protonated amine functionality. The hydridic and protic hydrogen atoms in **G** would then react to render a H_2 molecule and to regenerate **A**, as shown in Figure S28. Overall, the rate-determining transition state corresponds to $\mathbf{TS_{B\text{-}G}}$, which is translated into an energy span of 27.4 kcal·mol^{-1}. Notice that this mechanism would be competitive with the previous one (black lines), as there is an energy difference between $\mathbf{TS_{B\text{-}DF}}$ and $\mathbf{TS_{B\text{-}G}}$ of only 0.2 kcal·mol^{-1} (lower than the uncertainty of the calculations). Moreover, given the reaction temperature (50 °C), these mechanisms would be operative in the absence of cobaltate anion, leading to a slower, albeit non-negligible, reaction.

An alternative mechanism that entails the activation of methanol by the amine functionality has also been explored. However, such mechanism led to an effective span of 38.9 kcal·mol^{-1}, thus being discarded (see Figure S28). At this point, it is important to highlight that we also explored the possibility of CO dissociation rather than the amine moiety (see Figure S29). The resulting reaction intermediate, denoted as **B'**, is close in energy to **B**, with relative Gibbs energies of 17.4 and 16.6 kcal·mol^{-1}, respectively. However, the associated transition state without the CO ligand, $\mathbf{TS_{B\text{-}CD}'}$, displays a significantly higher Gibbs energy (39.7 vs. 22.8 kcal·mol^{-1}, respectively). As a result, this alternative was discarded.

In this line, we considered the possibility of the hydrosilane oxidative addition to the Co(I) center as the first reaction step, which is closely related with the reaction mechanism proposed for **3** (vide infra). Nonetheless, we found that the silane oxidative addition product (denoted as **B''**) has a relative Gibbs energy of 22.4 kcal·mol^{-1}, comparable to that of $\mathbf{TS_{B\text{-}CD}}$ (22.8 kcal·mol^{-1}), which is too high for a reaction intermediate (see Figure S30). Moreover, we calculated a transition state ($\mathbf{TS_{B''\text{-}A}}$) that yields the siloxane product and **A** directly from **B''** (in line to that proposed for **3**), and has a relative Gibbs energy of 46.0 kcal·mol^{-1} (and requires the decoordination of a CO ligand). Therefore, this alternative was also discarded.

In summary, the comprehensive evaluation of plausible mechanisms for the methanolysis of $PhSiH_3$ catalyzed by **1** suggest that the Co(I)/Co(–I) complex acts as a transition metal frustrated Lewis pair (TMFLP), which is capable of promoting the heterolytic activation of the Si–H bond. It is remarkable to note that bimetallic complexes that act as FLPs have emerged as a promising alternative to

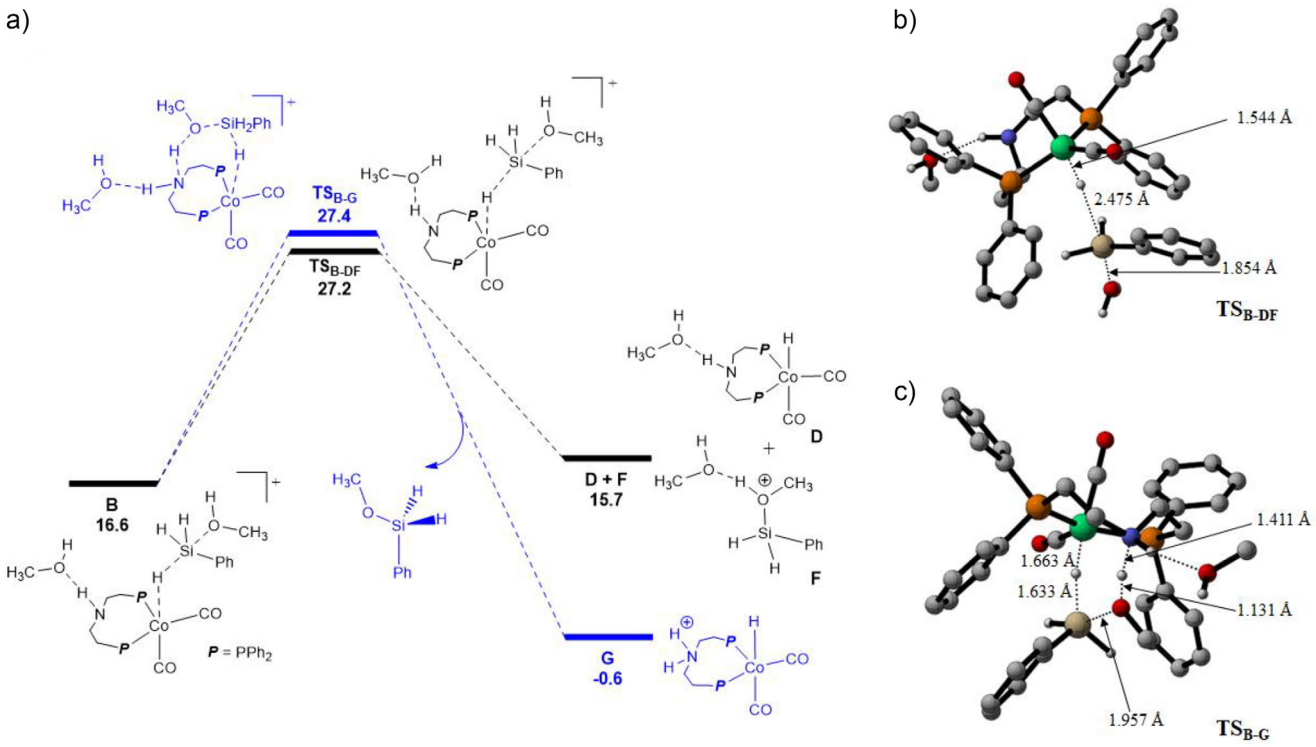

Figure 7. a) First part of the alternative reaction mechanism for the methanolysis of $PhSiH_3$ (in kcal·mol^{-1}) relative to **A**; b) **TS$_{B-DF}$**; and c) **TS$_{B-G}$**. Nonrelevant hydrogen atoms in b) and c) have been omitted for clarity.

boost the bond activation capabilities of transition metal catalysts, with the main examples comprising heterobimetallic systems.[71–73] This catalyst instead involves Lewis acid and Lewis basic centers, both based on cobalt, Co(I) and Co(–I), respectively.

In order to find further experimental support for the FLP behavior of **1** substantiated by DFT calculations, we prepared complex **4** ([Co(CO)$_2$(κ^3-*P*,*N*,*P*-PN^{H}P)]Cl) according to the procedure previously described by Zhou's group.[48] This catalyst is analogous to **1**, but it presents Cl^- as counterion instead of $[Co(CO)_4]^-$, thus excluding the possibility of an FLP pathway. The evaluation of the catalytic activity of **4** against **1** demonstrates a remarkably higher activity for the latter (Figure 8), which agrees with DFT calculations and the proposed FLP mechanism for **1**.

Initial TOF values decrease from 41 970 h^{-1} for **1** to 3310 h^{-1} for **4**. Furthermore, recycling experiments show a sharp decay of the catalytic activity for **4** in the second and third runs.

We also tested the activity of $[Co_2(CO)_8]$, as the dinuclear heterolytic splitting of the Si–H bond by this complex, to give $[R_3SiCo(CO)_4]$ and $[HCo(CO)_4]$, has been reported—thus indicating its potential as a catalyst for the methanolysis of silanes, possibly operating via a mechanism reminiscent of that of **1**.[74] Remarkably, $[Co_2(CO)_8]$ is a competent catalyst; however, it is significantly less active than **1**, and rapid deactivation is observed—likely due to the absence of ligand stabilization. In this vein, the reaction of **1** with excess silane in CD_3CN, leads to the formation of H_2 and Si–Si adducts via dehydrogenative coupling,[49] along with changes

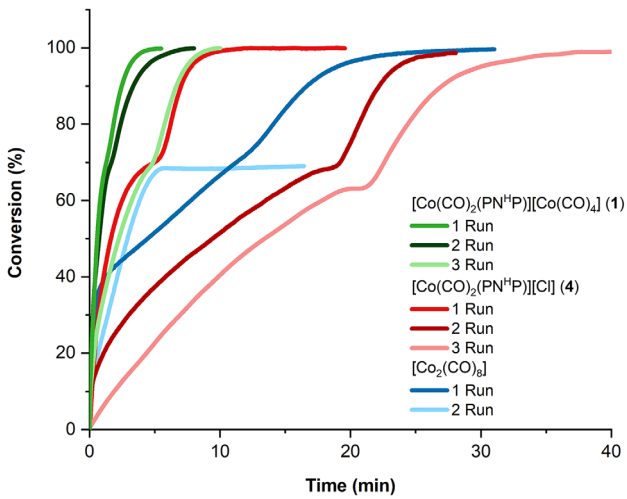

Figure 8. Conversion over time for the methanolysis of $PhSiH_3$ with catalysts **1**, **4**, and $Co_2(CO)_8$. Reaction conditions: 1 mol% of catalyst, 0.5 mmol of $PhSiH_3$, and 0.5 mL of MeOH at 50 °C.

in the ^1H and ^{31}P NMR spectra of **1**. Moreover, traces of a hydride complex are observed in the reaction mixture. This reactivity is consistent with that described for $[Co_2(CO)_8]$ with excess silane, where $[HCo(CO)_4]$ evolves to afford H_2 and $[Co_2(CO)_8]$, thereby serving as an indirect probe for the formation of a cobalt hydride complex.[74]

In an attempt to evaluate the importance of the NH moiety in **1**, we prepared and fully characterized the related

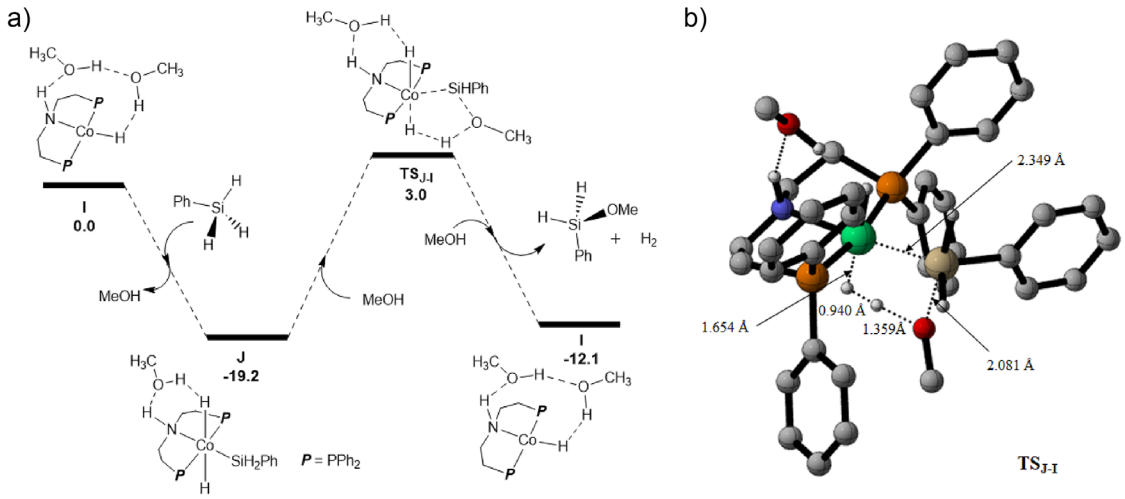

Figure 9. a) DFT calculated Gibbs energy profile for the methanolysis of $PhSiH_3$ (in kcal·mol^{-1}) relative to **I** and the isolated molecules; b) **TS$_{J\text{-}I}$**. Nonrelevant hydrogen atoms in b) have been omitted for clarity.

complex $[Co(CO)_2(\kappa^3\text{-}P,N,P\text{-}PN^{Me}P)][Co(CO)_4]$ (**5**), in which the nitrogen atom bears a methyl group instead of a proton (see Supporting Information). Complex **5** also exhibits good catalytic activity, indicating that the presence of an NH moiety is not essential for catalysis. However, a somewhat lower catalytic activity has been observed (Figure S47). This difference can be rationalized based on the proposed reaction mechanism (vide supra). To reach **TS$_{B\text{-}CD}$**, the nitrogen atom must decoordinate from the complex. In this context, the NH group in **1** facilitates this process by forming a hydrogen bond with a methanol molecule, thereby weakening the Co─N bond. This effect is switched off when the hydrogen atom is replaced by a methyl group. Additionally, the limited solubility of complex **5** in methanol is likely to impact its catalytic performance.

The association tendency of the Lewis acid (LA) and Lewis base (LB) in FLPs is thought to be important for FLP activity.[75,76] Therefore, ^{1}H DOSY (Diffusion-Ordered Spectroscopy) NMR was used to probe the ion pairing behavior of **1**.[77–79] The diffusion coefficients (D) of **1** in C_6D_6 and CD_3CN were calculated at 300 K, obtaining values of $5.428{\cdot}10^{-10}$ and $1.241{\cdot}10^{-9}$ m^2·s^{-1}, respectively. The average hydrodynamic radii (r_H) of **1** in C_6D_6 and CD_3CN were calculated by applying a modified Stokes─Einstein equation, resulting in values of 6.7 and 5.3 Å, respectively. The smaller diffusion coefficient and larger r_H in C_6D_6 agree with stronger LA···LB interactions in the nonpolar solvent, which confirms the formation of ion pairs of **1** in solution.

We then explored the reaction mechanism induced by catalyst **3**, since an alternative pathway is to be expected in this case. Based on experimental observations (vide supra), **3** is expected to undertake several chemical transformations that lead to a neutral hydride intermediate, which will be referred to as **I**. The proposed reaction mechanism is provided in Figure 9.

The initial step involves the oxidative addition of the silane to the Co(I) center in **I**, resulting in the formation of the octahedral Co(III) intermediate **J**. This process is highly favored from a thermodynamic perspective, with **J** exhibiting a Gibbs energy 19.2 kcal·mol^{-1} lower than that of **I**. Although a transition structure for this step could not be identified, barrierless oxidative additions of hydrosilanes are not unprecedented.[80]

Additionally, experimental observations support the formation of **J**, which further reinforces the validity of this reaction pathway. It is also illustrative to compare this behavior with that exhibited by **A**, where oxidative addition did not occur. In general terms, such difference in reactivity can be attributed to the presence of two CO ligands in **A**, which act as π-acceptors, thus withdrawing electronic density from the metal and destabilizing the oxidized Co(III) center. Therefore, although a vacant coordination site can be generated in **A** upon dissociation of the NH moiety of the PN^HP ligand, the oxidative addition of the Si─H bond is disfavored.

The subsequent step involves a concerted mechanism in which **J** reacts with a methanol molecule, releasing the final products (molecular hydrogen and the desired siloxane), and simultaneously undergoing the reduction to the monohydride Co(I) complex **I**, thereby closing the catalytic cycle. This step proceeds via **TS$_{J\text{-}I}$** (Figure 9b), which features a relative Gibbs energy of 3.0 kcal·mol^{-1}, and translates into an energy span of 22.2 kcal·mol^{-1}. Note that the overall ΔG of the cycle is −12.1 kcal·mol^{-1}, thus being favored from a thermodynamic point of view; nonetheless, the last step is endergonic by 7.1 kcal·mol^{-1}, which correlates with the observed high stability of **J**.

Kinetic isotope effect (KIE) experiments were conducted to gain a deeper understanding of the mechanisms that operate for catalysts **1** and **3** (Table 1). These experiments were carried out under the standard reaction conditions described above, employing Ph_2SiH_2 as hydrosilane.

In the case of **1**, the use of Ph_2SiD_2 leads to a KIE of 1.9. In stark contrast, no KIE was observed for **3** when

Table 1: KIE experiments conducted with catalysts **1** and **3** for the methanolysis of Ph_2SiH_2. Reaction conditions: catalyst (1 mol%), 0.5 mmol of Ph_2SiH_2 or Ph_2SiD_2, and 0.5 mL MeOH or MeOD at 50 °C.

Entry	Catalyst	[D]	KIE
1	**1**	Ph_2SiD_2	1.9
2	**3**	Ph_2SiD_2	1.0
3	**3**	MeOD	2.4

deuterated silane (Ph_2SiD_2) was used, which suggests that the splitting of the Si─H bond is not involved in the transition state, in agreement with DFT calculations. This prompted us to conduct the reaction in MeOD, which resulted in a noticeable reduction of the reaction rate, resulting in a KIE of 2.4. These data also agree with the DFT calculations, as the splitting of the O─H bond of methanol takes place in the TOF-determining transition state ($\mathbf{TS_{J\text{-}1}}$).

Conclusion

We have described a straightforward method for the preparation of the bimetallic Co(I)/Co(–I) complex **1**. The catalytic activity of **1** in the methanolysis and hydrolysis of silanes was evaluated, this being the first example of a well-defined Co(I) catalyst for these transformations. Remarkably, **1** is more active than the related Co(II) complex **3** despite the fact that the latter presents more accessible coordination sites upon in situ reduction to the Co(I) active species. This behavior has been ascribed to the presence of the $[Co(CO)_4]^-$ anion, which allows for a frustrated Lewis pair mechanism, resulting in a low energy pathway for the heterolytic splitting of the Si─H bond, as substantiated by DFT calculations. Further proof for this mechanism is the comparatively lower activity observed for complex **4** ($[Co(CO)_2(\kappa^3\text{-}P,N,P\text{-}PN^HP)]Cl$), which is analogous to **1**, but presents a Cl^- counterion instead of $[Co(CO)_4]^-$. Therefore, neither the Luo-Crabtree nor a NH-assisted bifunctional mechanism operate in this case, thus illustrating the mechanistic wealth that arises from subtle modifications of the structure of the cobalt catalyst.

Acknowledgements

Grants PID2021-126212OB-I00 and PID2021-122763NB-I00 funded by MCIN/AEI/10.13039/501100011033 and by "ERDF A way of making Europe", as well as the "Departamento de Ciencia, Universidad y Sociedad del Conocimiento del Gobierno de Aragón" (group E42_23R) and Fundación Ibercaja and Universidad de Zaragoza (grant JIUZ2023-CIE-10) are gratefully acknowledged. D.B.-E. also acknowledges Spanish "Fundación para el Fomento en Asturias de la Investigación Científica Aplicada y la Tecnología" (Grant No. PA-23-BP22-168). A. L.-G. gratefully acknowledges the MCIN for the predoctoral grant PRE2019-087598. Authors would like to acknowledge the use of Servicio General de Apoyo a la Investigación-SAI at the Universidad de Zaragoza and at the ISQCH/CEQMA (CSIC).

Conflict of Interests

The authors declare no conflict of interest.

Data Availability Statement

The data that support the findings of this study are available in the Supporting Information of this article.

Keywords: Catalysis · Cobalt · Frustrated Lewis pairs · Hydrogen storage · Reaction mechanism

[1] I. Ojima, Z. Li, J. Zhu, in *PATAIS Chem. Funct. Groups* (Eds: Z. Rappoport, Y. Apeloig) Wiley, New York, pp. 1687–1792.
[2] V. Chandrasekhar, R. Boomishankar, S. Nagendran, *Chem. Rev.* **2004**, *104*, 5847–5910.
[3] S. E. Denmark, C. S. Regens, *Acc. Chem. Res.* **2008**, *41*, 1486–1499.
[4] J. C. Furgal, C. U. Lenora, *Phys. Sci. Rev.* **2020**, *5*, 20190024.
[5] W.-S. Han, T.-J. Kim, S.-K. Kim, Y. Kim, Y. Kim, S.-W. Nam, S. O. Kang, *Int. J. Hydrog. Energy* **2011**, *36*, 12305–12312.
[6] N. Asao, Y. Ishikawa, N. Hatakeyama, Menggenbateer, Y. Yamamoto, M. Chen, W. Zhang, A. Inoue, *Angew. Chem. Int. Ed.* **2010**, *49*, 10093–10095.
[7] K. Shimizu, T. Kubo, A. Satsuma, *Chem. – Eur. J.* **2012**, *18*, 2226–2229.
[8] J. John, E. Gravel, A. Hagège, H. Li, T. Gacoin, E. Doris, *Angew. Chem. Int. Ed.* **2011**, *50*, 7533–7536.
[9] W. Li, A. Wang, X. Yang, Y. Huang, T. Zhang, *Chem. Commun.* **2012**, *48*, 9183.
[10] Y. Kikukawa, Y. Kuroda, K. Yamaguchi, N. Mizuno, *Angew. Chem. Int. Ed.* **2012**, *51*, 2434–2437.
[11] M. Jeon, J. Han, J. Park, *ChemCatChem* **2012**, *4*, 521–524.
[12] Y. Wang, X.-K. Wan, L. Ren, H. Su, G. Li, S. Malola, S. Lin, Z. Tang, H. Häkkinen, B. K. Teo, Q.-M. Wang, N. Zheng, *J. Am. Chem. Soc.* **2016**, *138*, 3278–3281.
[13] T. Mitsudome, T. Urayama, T. Kiyohiro, Z. Maeno, T. Mizugaki, K. Jitsukawa, K. Kaneda, *Sci. Rep.* **2016**, *6*, 37682.
[14] N. Almenara, M. A. Garralda, X. Lopez, J. M. Matxain, Z. Freixa, M. A. Huertos, *Angew. Chem.* **2022**, *134*, e202204558.
[15] X. L. Luo, R. H. Crabtree, *J. Am. Chem. Soc.* **1989**, *111*, 2527–2535.
[16] L. D. Field, B. A. Messerle, M. Rehr, L. P. Soler, T. W. Hambley, *Organometallics* **2003**, *22*, 2387–2395.
[17] D. Ventura-Espinosa, S. Sabater, A. Carretero-Cerdán, M. Baya, J. A. Mata, *ACS Catal.* **2018**, *8*, 2558–2566.
[18] K. Garcés, F. J. Fernández-Alvarez, V. Polo, R. Lalrempuia, J. J. Pérez-Torrente, L. A. Oro, *ChemCatChem* **2014**, *6*, 1691–1697.
[19] M. Aliaga-Lavrijsen, M. Iglesias, A. Cebollada, K. Garcés, N. Garciá, P. J. Sanz Miguel, F. J. Fernández-Alvarez, J. J. Pérez-Torrente, L. A. Oro, *Organometallics* **2015**, *34*, 2378–2385.
[20] I. Pappas, S. Treacy, P. J. Chirik, *ACS Catal.* **2016**, *6*, 4105–4109.
[21] M. L. Scheuermann, E. J. Johnson, P. J. Chirik, *Org. Lett.* **2015**, *17*, 2716–2719.
[22] J. V. Obligacion, P. J. Chirik, *J. Am. Chem. Soc.* **2013**, *135*, 19107–19110.
[23] L. Zhang, Z. Zuo, X. Wan, Z. Huang, *J. Am. Chem. Soc.* **2014**, *136*, 15501–15504.
[24] B. Raya, S. Jing, V. Balasanthiran, T. V. RajanBabu, *ACS Catal.* **2017**, *7*, 2275–2283.
[25] Z.-Y. Zhao, Y.-X. Nie, R.-H. Tang, G.-W. Yin, J. Cao, Z. Xu, Y.-M. Cui, Z.-J. Zheng, L.-W. Xu, *ACS Catal.* **2019**, *9*, 9110–9116.

[26] W. N. Palmer, T. Diao, I. Pappas, P. J. Chirik, *ACS Catal.* **2015**, *5*, 622–626.
[27] B. Raya, S. Biswas, T. V. RajanBabu, *ACS Catal.* **2016**, *6*, 6318–6323.
[28] C. C. Bories, M. Barbazanges, E. Derat, M. Petit, *ACS Catal.* **2021**, *11*, 14262–14273.
[29] C. C. Bories, A. Sodreau, M. Barbazanges, M. Petit, *Organometallics* **2024**, *43*, 895–923.
[30] A. L. Amaya, H. Alawisi, H. D. Arman, Z. J. Tonzetich, *Organometallics* **2023**, *42*, 2902–2909.
[31] S. Pattanaik, C. Gunanathan, *ACS Catal.* **2019**, *9*, 5552–5561.
[32] M. Hamdaoui, M. Ney, V. Sarda, L. Karmazin, C. Bailly, N. Sieffert, S. Dohm, A. Hansen, S. Grimme, J.-P. Djukic, *Organometallics* **2016**, *35*, 2207–2223.
[33] E. Szafoni, K. Kuciński, G. Hreczycho, *Green Chem. Lett. Rev.* **2022**, *15*, 757–764.
[34] P. Guo, L.-C. Cheng, X. He, K.-Y. Ye, *Org. Chem. Front.* **2022**, *9*, 5802–5807.
[35] T. Li, H. Zhang, A. S. C. Chan, S.-S. Meng, *Cell Rep. Phys. Sci.* **2023**, *4*, 101313.
[36] E. Antico, M. Leutzsch, N. Wessel, T. Weyhermüller, C. Werlé, W. Leitner, *Chem. Sci.* **2023**, *14*, 54–60.
[37] A. K. Liang Teo, W. Y. Fan, *Chem. Commun.* **2014**, *50*, 7191–7194.
[38] W. Sattler, G. Parkin, *J. Am. Chem. Soc.* **2012**, *134*, 17462–17465.
[39] Z. Han, L. Rong, J. Wu, L. Zhang, Z. Wang, K. Ding, *Angew. Chem. Int. Ed.* **2012**, *51*, 13041–13045.
[40] S. Kar, A. Goeppert, G. K. S. Prakash, *Acc. Chem. Res.* **2019**, *52*, 2892–2903.
[41] S.-T. Bai, C. Zhou, X. Wu, R. Sun, B. Sels, *ACS Catal.* **2021**, *11*, 12682–12691.
[42] Q. Liu, L. Wu, S. Gülak, N. Rockstroh, R. Jackstell, M. Beller, *Angew. Chem. Int. Ed.* **2014**, *53*, 7085–7088.
[43] S. Kar, R. Sen, J. Kothandaraman, A. Goeppert, R. Chowdhury, S. B. Munoz, R. Haiges, G. K. S. Prakash, *J. Am. Chem. Soc.* **2019**, *141*, 3160–3170.
[44] P. A. Dub, J. C. Gordon, *Nat. Rev. Chem.* **2018**, *2*, 396–408.
[45] E. A. Bielinski, P. O. Lagaditis, Y. Zhang, B. Q. Mercado, C. Würtele, W. H. Bernskoetter, N. Hazari, S. Schneider, *J. Am. Chem. Soc.* **2014**, *136*, 10234–10237.
[46] E. Alberico, P. Sponholz, C. Cordes, M. Nielsen, H. Drexler, W. Baumann, H. Junge, M. Beller, *Angew. Chem. Int. Ed.* **2013**, *52*, 14162–14166.
[47] M. Andérez-Fernández, L. K. Vogt, S. Fischer, W. Zhou, H. Jiao, M. Garbe, S. Elangovan, K. Junge, H. Junge, R. Ludwig, M. Beller, *Angew. Chem. Int. Ed.* **2017**, *56*, 559–562.
[48] W. Zhou, Z. Wei, A. Spannenberg, H. Jiao, K. Junge, H. Junge, M. Beller, *Chem. – Eur. J.* **2019**, *25*, 8459–8464.
[49] A. Luque-Gómez, P. García-Orduña, F. J. Lahoz, M. Iglesias, *Dalton Trans.* **2023**, *52*, 12779–12788.
[50] A. W. Addison, T. N. Rao, J. Reedijk, J. Van Rijn, G. C. Verschoor, *J. Chem. Soc. Dalton Trans.* **1984**, *7*, 1349–1356.
[51] M. R. Mills, C. L. Barnes, W. H. Bernskoetter, *Inorg. Chem.* **2018**, *57*, 1590–1597.
[52] L. Brammer, *J. Organomet. Chem.* **2000**, *609*, 36–43.
[53] L. Brammer, J. C. Mareque Rivas, D. Zhao, *Inorg. Chem.* **1998**, *37*, 5512–5518.
[54] X. Liu, L. Longwitz, B. Spiegelberg, J. Tönjes, T. Beweries, T. Werner, *ACS Catal.* **2020**, *10*, 13659–13667.
[55] T. Edlová, A. T. Normand, H. Cattey, S. Brandès, Y. Wu, A. Antonangelo, B. Théron, Q. Bonnin, M. Carta, P. L. E. Gendre, *Organometallics* **2023**, *42*, 1166–1178.
[56] M. Tanabe, A. Takahashi, T. Fukuta, K. Osakada, *Organometallics* **2013**, *32*, 1037–1043.
[57] V. K. Dioumaev, R. M. Bullock, *Nature* **2003**, *424*, 530–532.
[58] D. V. Gutsulyak, S. F. Vyboishchikov, G. I. Nikonov, *J. Am. Chem. Soc.* **2010**, *132*, 5950–5951.
[59] D. V. Gutsulyak, G. I. Nikonov, *Angew. Chem. Int. Ed.* **2010**, *49*, 7553–7556.
[60] S. Rendler, M. Oestreich, *Angew. Chem. Int. Ed.* **2008**, *47*, 5997–6000.
[61] D. V. Gutsulyak, A. van der Est, G. I. Nikonov, *Angew. Chem.* **2011**, *123*, 1420–1423.
[62] S. Park, M. Brookhart, *Organometallics* **2010**, *29*, 6057–6064.
[63] T. T. Metsänen, D. Gallego, T. Szilvási, M. Driess, M. Oestreich, *Chem. Sci.* **2015**, *6*, 7143–7149.
[64] D. J. Parks, J. M. Blackwell, W. E. Piers, *J. Org. Chem.* **2000**, *65*, 3090–3098.
[65] D. J. Parks, W. E. Piers, *J. Am. Chem. Soc.* **1996**, *118*, 9440–9441.
[66] J. Fuchs, H. F. T. Klare, M. Oestreich, *ACS Catal.* **2017**, *7*, 8338–8342.
[67] J. A. R. Schmidt, E. B. Lobkovsky, G. W. Coates, *J. Am. Chem. Soc.* **2005**, *127*, 11426–11435.
[68] J. Zhao, P. Wu, E. Lai, J. Li, Y. Chen, W. Jiang, B. Wang, H. Zhu, *Chem. – Asian J.* **2021**, *16*, 3453–3461.
[69] Y. Wen, R. Nie, B. Li, S. Li, *ACS Catal.* **2023**, *13*, 3317–3322.
[70] F.-G. Deng, B. Hu, W. Sun, J. Chen, C.-G. Xia, *Dalton Trans.* **2007**, 4262–4267.
[71] J. Campos, *J. Am. Chem. Soc.* **2017**, *139*, 2944–2947.
[72] N. Hidalgo, J. J. Moreno, M. Pérez-Jiménez, C. Maya, J. López-Serrano, J. Campos, *Chem. – Eur. J.* **2020**, *26*, 5982–5993.
[73] N. Hidalgo, J. J. Moreno, M. Pérez-Jiménez, C. Maya, J. López-Serrano, J. Campos, *Organometallics* **2020**, *39*, 2534–2544.
[74] A. J. Chalk, J. F. Harrod, *J. Am. Chem. Soc.* **1965**, *87*, 1133–1135.
[75] L. Rocchigiani, G. Ciancaleoni, C. Zuccaccia, A. Macchioni, *J. Am. Chem. Soc.* **2014**, *136*, 112–115.
[76] A. J. V. Marwitz, J. L. Dutton, L. G. Mercier, W. E. Piers, *J. Am. Chem. Soc.* **2011**, *133*, 10026–10029.
[77] P. S. Pregosin, *Prog. Nucl. Magn. Reson. Spectrosc.* **2006**, *49*, 261–288.
[78] T. Wiegand, H. Eckert, O. Ekkert, R. Fröhlich, G. Kehr, G. Erker, S. Grimme, *J. Am. Chem. Soc.* **2012**, *134*, 4236–4249.
[79] O. J. Metters, S. J. K. Forrest, H. A. Sparkes, I. Manners, D. F. Wass, *J. Am. Chem. Soc.* **2016**, *138*, 1994–2003.
[80] J. N. P. Van Stralen, F. M. Bickelhaupt, *Organometallics* **2006**, *25*, 4260–4268.

Manuscript received: June 20, 2025
Revised manuscript received: July 02, 2025
Accepted manuscript online: July 02, 2025
Version of record online: ■■, ■■

Research Article

Cobalt Catalysis

A. Luque-Gómez, D. Barrena-Espés, P. García-Orduña, A. Pérez-García, M. A. Casado, J. Munarriz*, M. Iglesias* ——— **e202513522**

A Homobimetallic Frustrated Lewis Pair Cobalt Catalyst for the Methanolysis of Hydrosilanes

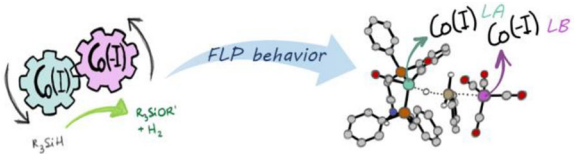

The bimetallic Co(I)/Co(–I) complex $[Co(CO)_2(\kappa^3\text{-}P,N,P\text{-}PN^HP)][Co(CO)_4]$ shows excellent activities in the methanolysis of hydrosilanes, reaching TOF values of ca. 50 000 h^{-1}. This behavior can be ascribed to the presence of the $[Co(CO)_4]^-$ anion, which allows for a frustrated Lewis pair mechanism, resulting in a low energy pathway for the heterolytic splitting of the Si—H bond, as substantiated by DFT calculations.